Review of optical properties of two-dimensional transition metal dichalcogenides

Conference Paper · September 2018

DOI: 10.1117/12.2323132

3 authors, including:

Andrew Voshell
Delaware State University
6 PUBLICATIONS **33** CITATIONS
SEE PROFILE

Mukti Rana
Delaware State University
28 PUBLICATIONS **133** CITATIONS
SEE PROFILE

Review of optical properties of two-dimensional transition metal dichalcogenides

Andrew Voshell, Mauricio Terrones, Mukti Rana

Andrew Voshell, Mauricio Terrones, Mukti Rana, "Review of optical properties of two-dimensional transition metal dichalcogenides," Proc. SPIE 10754, Wide Bandgap Power and Energy Devices and Applications III, 107540L (7 September 2018); doi: 10.1117/12.2323132

SPIE.

Event: SPIE Optical Engineering + Applications, 2018, San Diego, California, United States

Review of optical properties of two-dimensional transition metal dichalcogenides

Andrew Voshell[a], Mauricio Terrones[b] and Mukti Rana[a]

[a]Department of Physics and Engineering and Optical Science Center for Applied Research, Delaware State University, Dover, DE 19901, USA
[b]Department of Physics, Chemistry and Materials Science & Engineering, Pennsylvania State University, University Park, PA 16802, USA

ABSTRACT

Two dimensional (2D) materials have become a growing subject in the last 15 years mainly due to the isolation of graphene, which created a completely different class of material based on its unique, monolayer design. Since then, various stable materials of few atoms thick are showing emerging capabilities in optical electronics and photonics. Semiconducting monolayers of transition metal dichalcogenides (TMDs) such as MoS_2, $Mo_{1-x}W_xS_2$, and WS_2 exhibit direct electronic band gaps; bulk crystals display indirect band gaps. Interestingly, these 2D materials show significant light interaction over a broad bandwidth ranging from infrared to ultraviolet wavelengths. The materials allow photodetection in this bandwidth without the need of cooling, thus creating new potential for uncooled detection. In this review, we discuss various 2D materials and their interaction with light for photodetection applications.

Keywords: Transition metal dichalcogenides, semiconductor, optical properties, photoluminescence, photodetector, band gap, two-dimensional, absorbance

1. INTRODUCTION

Scientific advancements in two-dimensional (2D) materials, notably the isolation and properties of graphene in 2004 [1], has led to wide interest in using 2D materials for various optoelectronic applications. Since then, many other bi-dimensional materials have been fabricated and novel electrical and optical properties have been reported. Studies of these materials have led to a new genre of 2D semiconducting materials with unprecedented properties.

One of type of 2D material, transition metal dichalcogenides (TMDs), has become heavily studied in recent years due to their unique characteristics useful for optoelectronics [2]. TMDs are of the form MX_2, where M is a transition metal (Mo, W, etc.), and X is a dichalcogenide (S, Se, Te). Bulk TMD is composed of many stacked layers held together by weak van der Waals forces. The reduction in the number of layers in TMDs by exfoliation, or their synthesis by chemical vapor deposition (CVD) processes, allows single- or few-layer sheets to be made.

Many exciting electronic and optical properties can be found in 2D TMDs. One of them is the transformation from an indirect band gap semiconductor to a direct band gap semiconductor when the thickness of TMDs changes from several layers to a monolayer. This characteristic can provide unique advantages to the material, including an increased absorption and photoluminescence (PL) based on the layer number [2, 4]. Layer-dependent change in optical properties has also been heavily explored, allowing possibilities for tuning optical band gaps and PL emissions. In addition, stacked layers of different TMDs result in van der Waals solids with novel photodetector capabilities.

Due to the many combinations, structures, and properties possible in TMDs, in this paper we will limit the review to optical properties of mostly molybdenum and tungsten dichalcogenides (MoS_2, $MoSe_2$, $MoTe_2$, WS_2, WSe_2, WTe_2) and their alloys.

Wide Bandgap Power and Energy Devices and Applications III, edited by Mohammad Matin, Srabanti Chowdhury, Achyut K. Dutta, Proc. of SPIE Vol. 10754, 107540L · © 2018 SPIE · CCC code: 0277-786X/18/$18 · doi: 10.1117/12.2323132

2. LINEAR OPTICAL PROPERTIES

2.1 Optical Transitions:

Semiconducting TMDs have shown unique band and transition properties when they are reduced from bulk form to few- and mono-layer forms. Bulk and few-layer TMDs exhibit an indirect band gap, involving lattice vibrations (phonons) as well as optical transitions from the valence band to the conduction band. However, single-layer TMDs show a direct band gap transition, displaying large absorption when exciting with photon energies able to perform the transition.

Optical energy band gaps can be studied by photoluminescence (PL), which will be discussed below in depth, as well as Tauc's relation. The Tauc relationship can be expressed by the following equation [5]:

$$\alpha h\nu = A\left(h\nu = E_g\right)^n \tag{1}$$

Where, α is the absorption coefficient, A is a constant, $h\nu$ is photon energy, E_g is the band gap energy of the material, and describes the type of electronic transition. n can be 1/3, ½, 2/3 and 2 meaning indirect forbidden, indirect allowed, direct forbidden, and direct allowed, respectively. Plotting $(\alpha h\nu)^n$ versus $h\nu$ gives the Tauc plot, and by studying the linear portion of the plot along the $h\nu$ axis provides the optical band gap of the material.

Like the excitation of electrons when interacting with light in 2D TMDs, the radiative recombination, specifically the lifetime, is important to study in semiconductors. Control of the exciton dynamics of these materials can be very useful in detector system optimization. In this context, very few studies have been performed on the radiative lifetimes. Studies have found that the exciton radiative lifetime of monolayer TMDs are in the picosecond (1-10ps) range for low temperature (0-4K), and in the nanosecond (0.1-10ns) range for the room-temperature decay [6]. It has also been found that, in the TMDs studied, the radiative recombination in bulk and few-layers is slower than the lifetime of monolayer TMDs. For example, Kumar et al. [7] performed excitonic dynamics analysis on $MoSe_2$ monolayers and bulk materials, finding a decay rate of about 0.9ns. These authors also noticed that the bulk form has a decay time about twice as slow as the monolayer form. Palummo et al. [8] also showed exciton lifetimes for monolayer MoS_2, $MoSe_2$, WS_2, and WSe_2, as well as bilayer and bulk MoS_2 for low- and room-temperature excitations of the lowest energy absorption peak (A). They also noticed that in MoS_2, as the layer number increased from 1, 2 and bulk, the radiative lifetime increased for both room temperature and for 0K. This adds another degree of freedom in optoelectronic capabilities, as the exciton dynamics could be controlled and tuned for various applications.

2.1.1 MoX_2 compounds

Many studies have used the absorbance spectrum of direct and indirect transitions as well as the Tauc relationship to study the band gap properties of TMDs. Figure 1 shows the Tauc relation plotted with photon energy for MoS_2 and $MoTe_2$, and by extrapolating the linear portion of the indirect or direct transitions, it is possible to determine the optical band gap of the material. Michester et al. [9] performed liquid-phase exfoliation of bulk MoS_2 in order to reduce down to few- and mono-layer sheets. The authors found three excitation peaks A, B, and C in the absorbance spectra, and plotted $(\alpha E)^2$ against photon energy E. The peaks A, B, and C were due to exciton splitting, with values centered at 680nm, 620nm, and 455nm, respectively. The Tauc's plot linear extrapolation shows an optical band gap estimation of 1.75eV, which corresponds to flakes of about three to four layers.

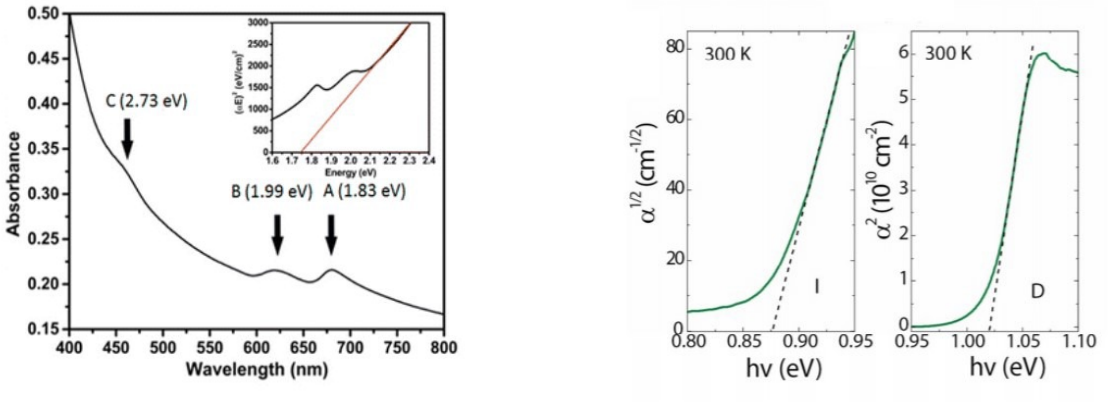

(a) (b)

Figure 1: Tauc plot measurements and linear portion extrapolation of a) MoS_2 using direct transition (n=2) [9] and b) $MoTe_2$ using both direct(n=2) and indirect (n=1/2) transition values [10].

Lezama et al. [10] performed absorption measurements on $MoTe_2$ films and plotted the Tauc's relationship to study the direct and indirect transition energy band gap. The authors plotted both the indirect (n=1/2) and direct (n=2) transitions of equation (1) and extrapolated the linear portion of the graphs. The group found an indirect band gap of about 0.875 eV and a direct band gap of about 1.03 eV.

2.1.2 WX compounds

Semiconducting tungsten dichalcogenides such as WS_2 and WSe_2 exhibit optical transition properties like molybdenum dichalcogenides, but with different transition energies in the bulk, few-layers, and monolayers. In this context, Morrish et al. [11] performed the Tauc's relation with an indirect transition (n=1/2) on the absorbance spectra for WS_2 films, showing an indirect band gap transition at about 1.4eV. The plot for their measurements is shown in figure 2(a). Yu et al. [12] performed optical absorbance measurements on solvent-exfoliated monolayer WSe_2 flakes. From figure 2(b), the authors extrapolated the linear portion of the Tauc's plot with a direct allowed transition (n=2), showing a direct band gap of about 1.75eV.

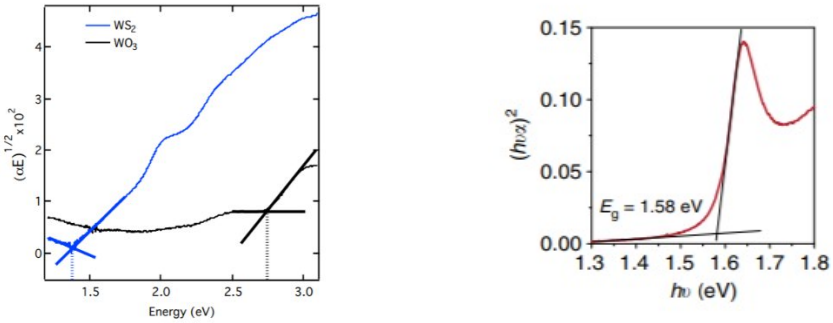

(a) (b)

Figure 2: Tauc plot and linear extrapolation on a) WS_2 thin films using indirect transition (n=1/2) [11], and b) WSe_2 monolayer flakes using direct transition (n=2) [12].

2.2 Absorbance

The optical interaction with light of direct band gap semiconductors is very important in optoelectronics. Absorption is proportional to the energy of the incident photons on the material and it is commonly represented as the percentage of light neither transmitted nor reflected, thus equal to $A = 1 - T - R$, where A, T, and R is the fractional absorbance, transmission, and reflection, respectively. However, in semiconductors, it is often useful to express the absorption as a function of the thickness, regarded as the absorption coefficient. The absorption coefficient α, from the Beer-Lambert Law can be expressed as [13]:

$$\alpha = \frac{2.303\left(\ln\left(\frac{1}{T}\right)\right)}{t} \tag{2}$$

where, t is the thickness of material the light has travelled through, and T is the transmittance of the material. The numerator of equation (2) refers to the logarithmic absorbance of light through a material, sometimes regarded as "optical depth". Thus α can be further simplified to $\alpha = \frac{A}{t}$.

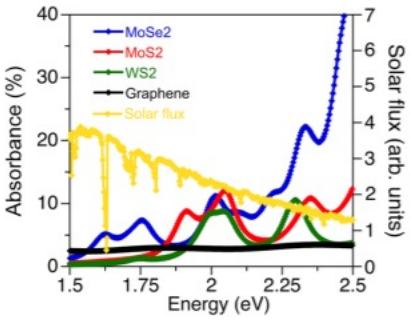

Figure 3: Fractional absorbance spectra of several TMDs over 1.5-2.5eV, including the absorbance of graphene and solar flux [17]

The absorbance of light in thinned layered materials on a thick substrate can also be found from the reflectance spectra acquired on a material. For a layered system such as TMDs for thicknesses $t<<\lambda$, the absorbance of the material is given by [14, 15]

$$A = \frac{1}{4}(n_s^2 - 1)\frac{\Delta R}{R} \tag{3}$$

Where n_s is the refractive index of the substrate, and $\frac{\Delta R}{R}$ is the reflectance contrast spectra, given by:

$$\frac{\Delta R}{R} = \frac{R_{TMD+S} - R_S}{R_S} \tag{4}$$

Where, R_{TMD+S} is the reflectance of the TMD (or other thin layered material) on the substrate, and R_S is the reflectance of the substrate. For exciton peak location and measurements, only the reflectance contrast is needed, since $\frac{\Delta R}{R}$ is proportional to absorbance of light in the material.

Graphene has shown absorbance of about 2.3% in the visible and NIR range. However, several monolayers of TMDs have shown much higher absorbance at bandgap resonances, which usually fall in the visible and NIR range. Absorbance up to >10% has been observed at excitonic resonances, and even higher for some shorter wavelengths, due to inter-band transitions [16]. Figure (3) shows the absorbance of three different TMD monolayers (MoS_2, $MoSe_2$, WS_2), compared to graphene for the photon energy of 1.5-2.5eV [17]. The graph shows that all three TMDs exhibit absorbance of up to 10% in some parts of visible spectrum, as well as over 30% absorbance of light for $MoSe_2$ at energies over 2.4eV, despite all of them being less than 1nm thick. To compare with other common photovoltaic materials, some TMD materials can absorb up to 10 times more incident sunlight than Si or GaAs [17].

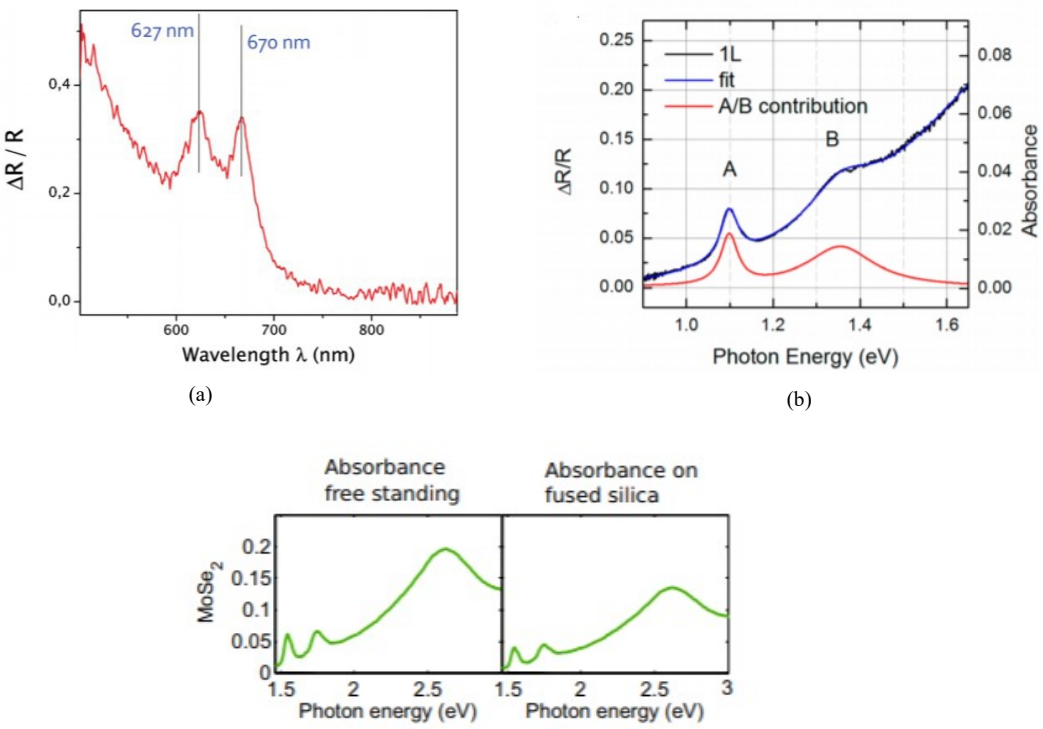

Figure 4: a) $\frac{\Delta R}{R}$ spectra for monolayer MoS_2 from 500-900nm wavelength [20] b) $\frac{\Delta R}{R}$ spectra and absorbance for monolayer $MoTe_2$ [21]. c) Absorbance spectra from monolayer $MoSe_2$ free standing and on fused silica [22]

The strong absorption of light in semiconducting monolayer TMDs is due to the light-matter interactions of the material. Peaks in TMD absorbance spectra are given by two interactions: band-edge excitons and excitons associated with the van Hove singularity [18,19]. Within the d orbitals of the transition metal atoms, the valence and conduction bands with energies close to the band gap, are composed of states. Dipole transitions with large joint density of states and oscillator strengths occur between these d orbitals [17].

2.2.1 MoX compounds:

All monolayers of molybdenum dichalcogenides display very strong absorption at excitation peaks. Two separate studies were performed by Splendiani et al. [20] and Ruppert et al. [21], to investigate the reflectance spectra using equation (4) on MoS_2 and $MoTe_2$, respectively. Splendiani et al. showed spectral data from 500-900nm (Figure 4a) for ultrathin exfoliated MoS_2 on a 280nm thick SiO_2 substrate. The reflectance contrast spectra showed two distinct absorption peaks located at 670nm and 627nm, corresponding to direct excitonic transitions at the Brillouin zone K point, known as A1 and B1 excitons in their work, respectively. Rupert et al. used mechanically exfoliated $MoTe_2$ monolayers deposited on SiO_2 substrates. The reflectance spectra in Figure 4(b) shows the excitonic peaks associated to the lowest direct optical transition at the K-point. The center point of the first exciton position (A) shows a direct band gap of 1.095 ± 0.005 eV [21]. This direct band gap shows promising optical capabilities in the NIR region, with an absorbance of about 3% at peak A and 4% at peak B.

Li et al. [22] performed mechanical exfoliation on bulk TMDs in order to produce few-layer sheets and measured optical absorbance on monolayers via a dielectric function technique, which was calculated by the reflectance spectra of the material. These authors showed the absorbance of monolayer $MoSe_2$ both free-standing and on a transparent fused silica substrate. They also found that free-standing monolayers showed strong absorbance peaks of about 5%, 5%, and 18% at exciton peaks A, B, and C, respectively, with a similar spectrum but lower value for the $MoSe_2$ on fused silica. For free-standing, the A and B peaks are centered at energies of about 1.57eV and 1.82eV, respectively, and correspond to the A and B excitons which are the smallest direct transitions at the K points in the Brillouin zone [23]. The C peak at high

energies is much broader spectrally with a peak at around 2.7eV, to which the broad response is due to higher-lying interband transitions near the Γ point [24].

2.2.2 WX_2 compounds

Semiconducting WX_2 monolayers such as WS_2 and WSe_2 have also shown high absorbance across the visible spectrum. In this context, Kozawa et al. [25] performed $\frac{\Delta R}{R}$ reflectance spectra on mechanically exfoliated monolayer WS_2 on a quartz between the photon energy of 1.6-2.8eV. The experimental absorbance data was calculated using equation (2) and plotted by reference [26] in Figure 5(a). The data shows strong absorbance of about 12% and 8% in the excitonic peaks A and B, respectively.

Similarly, He et al [27] performed both linear and nonlinear optical absorbance measurements on mechanically exfoliated monolayer WSe_2. For the linear regime, the group used reflectance contrast spectra on WSe_2 on a fused quartz substrate and used equation (3) to measure the absorbance of the material. Figure 5 (b) shows the calculated absorbance of the WSe_2 monolayer for photon energy 1.5-2.3eV. Two exciton peaks A and B were found at 1.65 and 2.3eV, respectively. The energy separation between A and B exciton states is about 0.43eV. This is due to strong spin-orbit coupling in WSe_2 and is very large compared to other TMDs [20,21,28].

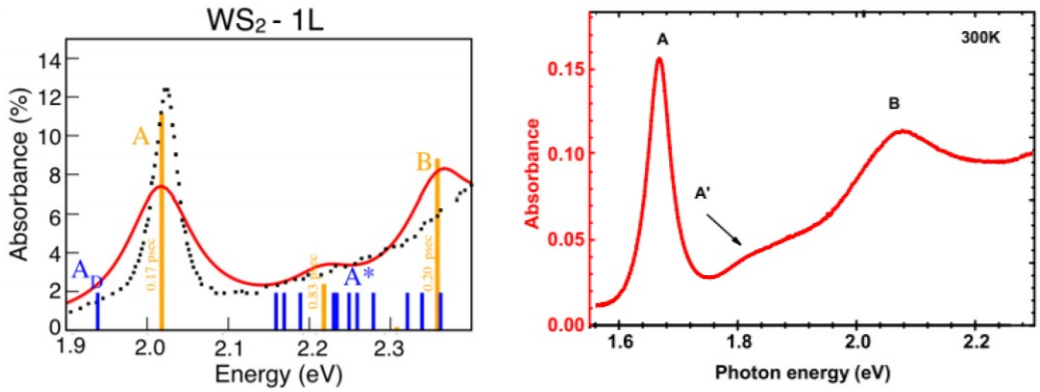

(a) (b)

Figure 5: a) Absorbance spectra of monolayer WS_2, data from reference [25], figure from reference [26] b) Absorbance spectra of monolayer WSe_2, with image reduced for clarity. [27]

In MoX_2 and WX_2 compounds, the choice of transition metals and chalcogen atoms can affect the absorption properties of the material. A red shift in the exciton peaks A and B is present in heavier chalcogen atoms, thus showing that the exciton absorption peaks occur at higher photon energies for Molybdenum and Tungsten sulfides than selenides. In addition, the interchanging of Mo and W atoms does not greatly affect the A exciton position. However, Yu et al. [58] reported that, when we replace Mo atom by W, the photon energy difference between the A and B exciton peaks increases. They found that by doing such interchange MoX_2 monolayers have an energy difference of 150meV and WX_2 monolayers have an energy difference of about 450meV [58]. This is due to the larger spin-orbit coupling of tungsten compared to molybdenum, which is intrinsic to the transition metal [3].

2.3 Luminescence

TMDs have shown unique band and transition properties as they reduce from the bulk form to few- and single-layer forms [2]. Bulk and few-layer TMDs have an indirect band gap, involving lattice vibrations (phonons) as well as energy transitions from the valence band to the conduction band. However, monolayer TMDs display a direct band gap transition, showing greater absorption as well as requiring only an incident photon energy to perform such a transition.

Spectroscopic ellipsometry, micro-Raman and photoluminescence (PL) measurements are usually used to determine the thickness as well as optical properties of TMDs. The interlayer interactions cause indirect (in bulk) to direct (in monolayer) bandgap transitions, which results in the reduction of the TMD layer thickness down to monolayer due to quantum confinement effects, band repulsion and localization, thereby making it optically active. The interlayer interactions are

contributed by Coulomb interactions between the transition metal ions and the chalcogenide ions in the adjacent layers, as understood from Raman spectroscopic studies. The surface relaxation effects in TMDs are also important, even though the interlayer interactions are weak. The indirect to direct band gap transition exists in all MX_2 when the number of layers decreases to monolayer. However, the specific distinct regimes with characteristic localization prototypes of band-edge states demonstrated strong material dependence.

2.3.1 MoX_2 compounds

Molybdenum dichalcogenides, which include MoS_2, $MoSe_2$, and $MoTe_2$, have shown strong PL properties in the visible and NIR regions. The band gap of these materials, in bulk form exhibit an indirect band gap that can range from about 0.9-1.3eV [21, 29, 61]. For monolayer forms of MoS_2, $MoSe_2$, and $MoTe_2$, all these materials display a direct band gap of 1-2eV [21, 28], respectively. The monolayer forms also have a very large PL emission efficiency, up to over 1,000 times higher than their bulk forms [28].

MoS_2 is the most extensively studied TMD in both its layered and monolayer form. Bulk MoS_2 has an indirect optical band gap of about 1.29 [59], and individual layers consist of covalently bonded hexagonal S and Mo atoms in a trigonal prismatic organization. PL spectra of few-layer MoS_2 has shown indirect band gap shift based on the layer number of the material, about 0.6eV from the bulk material [28]. the indirect band gap changes as the layers of the material changes and becomes a direct band gap of about 1.9 eV as a monolayer. In this context, Mak et al. [28] used mechanical exfoliation to create mono- and few-layer- crystals consisting of 1 to 6 layers. The authors performed optical absorption measurements, PL, and photoconductivity spectroscopy on their samples. For PL characteristics, an increase in quantum yield (QY) occurred as the number of layers were reduced from the bulk material to few layers. The monolayer MoS_2 showed a very large PL intensity, about 1000 times that of bulk material, due to the direct band gap of the monolayer. Figure 6 (b) shows the change in band gap energies as a function of layer number for layers 1-6, where layers 2-6 are determined by the peak of the indirect PL feature I, and 1-layer energy is at peak A (Figure 6 (a)).

Bulk $MoSe_2$ shares a similar crystal structure when compared to MoS_2, with a bulk indirect band gap in the near infrared of 1.09eV. Monolayer $MoSe_2$ has shown a direct optical band gap of 1.51eV. Here, Tonndorf et al. performed PL spectra for 1, 2, and 3-layer $MoSe_2$, shown in figure 6 (c) [29].

$MoTe_2$ is the heaviest and largest of the molybdenum dichalcogenides, with a bulk indirect band gap of about 1.0eV [30,31], and a monolayer direct band gap of about 1.1eV [21]. Ruppert et al. [21] showed through PL spectra of 1-5 layers of $MoTe_2$ in Figure 6 (d). Like other TMDs, the monolayer PL shows strong emissions, indicating a direct band gap, while layers 2-5 showed lower PL peaks that tended toward the bulk emissions as the layer number increased. Due to the small change in monolayer and the bulk optical band gap of $MoTe_2$, studies have found that the transformation from indirect to direct band gap may occur before the monolayer limit [32].

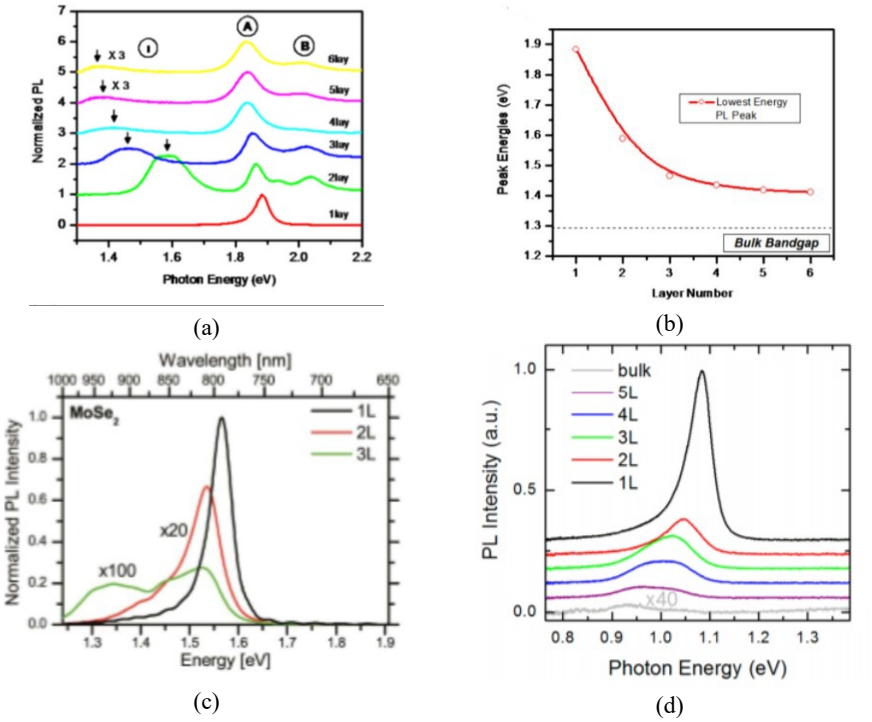

Figure 6: a) PL spectra of 1-6-layer MoS_2 [28]. b) Peak energy of PL spectra of MoS_2 as a function of layer number [28]. c) PL spectra of 1-3-layer $MoSe_2$ [29]. d) PL spectra of 1-5 layer and bulk $MoTe_2$ [21]

2.3.2 WX Compounds:

Tungsten dichalcogenides are another heavily studied form of TMDs, consisting of WS_2, WSe_2, and WTe_2. WS_2 and WSe_2 are both semiconductors in both bulk and monolayer form. The indirect optical band gap of these materials is very similar, with a value of about 1.2-1.3eV [21, 61]. However, the change in indirect band gap changes drastically when reduced to the few-layer form. Zhao et al. [33] measured the PL profile of WS_2 and WSe_2 for 1-5 layers. For WSe_2, there is a very small change between the indirect and direct peak energies in the PL spectra, showing the largest difference in these energies for 5 layers of about 0.2eV. However, WS_2 showed a much larger change in the indirect band gap as the number of layers increased, with the largest difference being about 0.6eV. Both WS_2 and WSe_2 displayed a linear increase in indirect peak emission as the number of layers decreased, with a single direct energy emission of 2eV and 1.65eV, respectively.

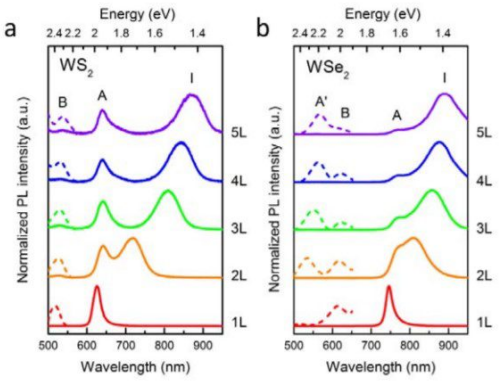

Figure 7: PL spectra for 1-5 layers of a) WS_2 and b) WSe_2. Both images are from reference [33]

WTe_2 is very different from other WX_2 compounds. The stable form of its atomic structure is octahedral, as opposed to the trigonal prismatic form of the other tungsten and molybdenum dichalcogenides [34]. However, this form of the material acts as a semimetal, with a small overlap between the CBM and VBM. The hexagonal form of the material does have a band gap of about 0.73eV, thus making it much narrower than other common TMDs [35]. The band gap was determined theoretically, thus no PL spectra has yet been performed on this material.

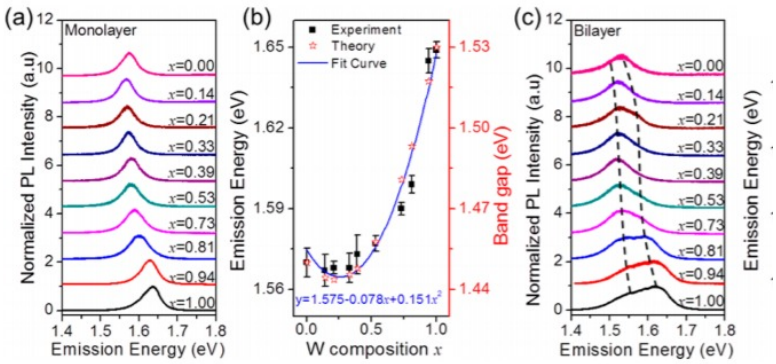

Figure 8: a) PL spectra of monolayer $Mo_{1-x}W_xSe_2$ for various composition values of x. b) Band gap value from PL spectra as a function of W composition (x). c) Bilayer PL spectra of $Mo_{1-x}W_xSe_2$ with various composition. All images from reference [36]

2.3.3 Alloys:

Along with the single TMD compounds, alloys such as $Mo_xW_{1-x}S_2$, $Mo_xW_{1-x}Se_2$, and $MoS_{2x}Se_{2(1-x)}$ have also been fabricated for specific PL tuning capabilities. By changing the composition of the monolayer material, continuous shift in PL emission peaks can be shown for $MoWSe_2$,

Zhang et al. performed PL and Raman scattering on several mechanically exfoliated $Mo_{1-x}W_xSe_2$ ($0 <= x <= 1$), monolayers and bilayer alloys [36]. The group noticed a shifted PL spectrum as the composition changed as well as a composition-dependent band gap emission which tuned from 1.56eV (at x = 0.21) to 1.65eV (at x = 1), shown in Figure 8(a) and (b). They also reported small but noticeable (20meV) emission peaks for the bilayer materials, which corresponds to the indirect and direct band gap exciton emissions.

OPTICAL DETECTORS

The ability to convert light into electrical signal is vital to a plethora of applications. Biomedical and video imaging, gas sensing, night-vision, motion detection, and optical communications, are all common uses of light sensors. This rapid increase in performance over the last few decades comes from the use of high-performance materials and development techniques. TMDs exhibit emergent optical properties, along with thinness, mechanical flexibility, and simple processing, makes them good candidates for specific photodetector applications. The band gap tunability and strong PL can allow these materials to cover a large range of novel applications in light absorption and emission technologies. In addition, and due to the intrinsic layered property of TMDs, they can be stacked forming heterostructures, and be incorporated with graphene and other layered material for optimal performance (see Figure 9 (d)).

Table 1: Optical band gap energies for semiconducting TMDs [21, 28, 29, 33, 59, 60, 61]

Material	Monolayer (direct) optical band gap (eV)	2 layer (indirect) optical band gap (eV)	3 layer (indirect) optical band gap (eV)	4 layer (indirect) optical band gap (eV)	5 layer (indirect) optical band gap (eV)	Bulk (indirect) optical band gap (eV)
MoS_2	1.9 [28]	1.6 [28]	1.47 [28]	1.44eV [28]	1.42 [28]	1.29 [59]
$MoSe_2$	1.57 [29]	1.54 [29]	1.53 [29]	-	-	1.1 [60]
$MoTe_2$	1.08 [21]	1.04 [21]	1.02 [21]	1.00 [21]	0.97 [21]	0.93 [21]
WS_2	1.97 [33]	1.71 [33]	1.53 [33]	1.46 [33]	1.42 [33]	1.3 [61]
WSe_2	1.65 [33]	1.53 [33]	1.44 [33]	1.42 [33]	1.39 [33]	1.2 [29]

Many qualities are involved in a good photodetector, such as responsivity, mobility, detectivity, and internal and external quantum efficiency [65]. Responsivity is one of the most important characteristics, which shows the electrical response of the detector under illumination. The equation for responsivity is usually expressed in AW^{-1} and is given by

$$R = \frac{I_{ph}}{P_{in}} \tag{5}$$

where I_{ph} is the photocurrent and P_{in} is the input optical power into the detector. Other parameters related to responsivity are important to describe the optical capabilities of these devices. External quantum efficiency (EQE) is the fraction of the number of electron-hole pairs generated per second to the number of photons incident on the detector per second. The equation for EQE is given by

$$EQE = \frac{hc}{e\lambda}R \tag{6}$$

Where h is planks constant, c is the speed of light in a vacuum, e is the elementary charge, and λ is the wavelength of the incident light. EQE is represented as a percentage but can exceed 100% because photon energy twice as much as the band gap of the material can generate two electron-hole pairs in the photoelectric process. In addition, cycling of the same electrons in a detector can attribute to a higher EQE [39].

Detectivity (D*) is related to responsivity, and it is a way to determine the performance of a photodetectors with different materials and sizes/shapes. The units for detectivity is in Jones ($cmHz^{1/2}/W$) and it is given by the equation:

$$D^* = \frac{\sqrt{A\Delta f}}{NEP} \tag{7}$$

Where A is the area of the device, Δf is the frequency bandwidth of the device, and NEP is the noise-equivalent power of the device. This value is the power of incident light that a detector can differentiate from noise of the device [39].

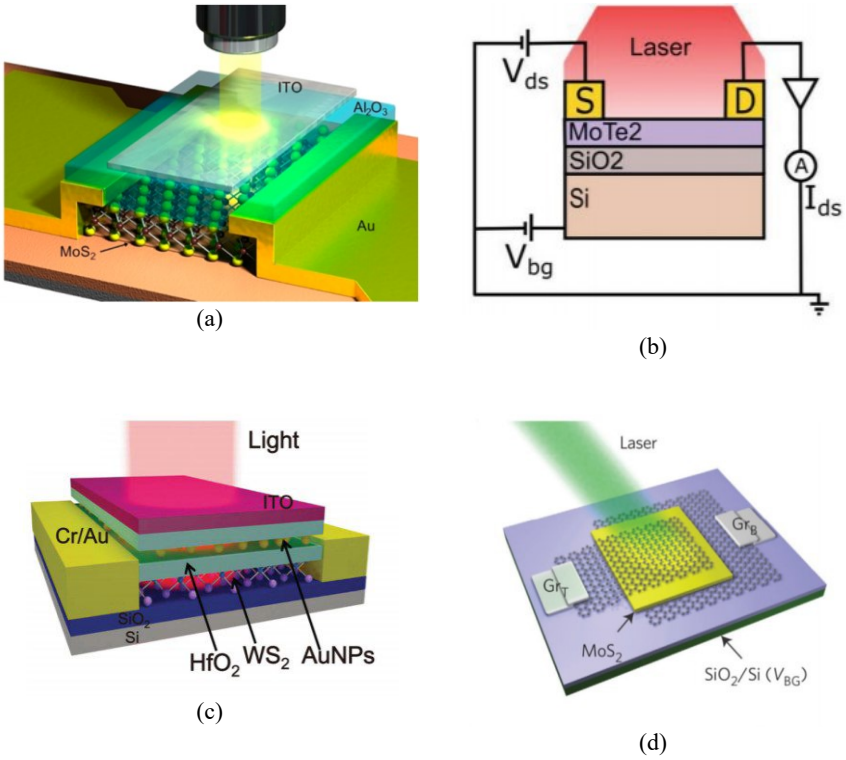

Figure 9: Various TMD-based photodetectors. a) an MoS_2-based photodetector diagram [37] b) Cross-sectional diagram of a $MoTe_2$-based photodetector [38] c) WS_2-based photodetector diagram with gold nanoparticle layer [63]. d) Diagram of a graphene-MoS_2-graphene heterostructure [62]

One of the first phototransistors fabricated and tested was by Yin et al. [40], who produced mechanically exfoliated MoS_2 on SiO2/Si substrates and found a responsivity of about 7.5 mA/W under illumination, with a response speed of 50ms. Although the responsivity was small when compared to Si or ZnO nanowires, it was already over seven times better than monolayer graphene-based FETs at the time (1mA/W). Due to optimized fabrication techniques and material choice, responsivity as well as the response time, has increased dramatically for 2D MoS_2-based devices. Huo et al. [41] recently produced an ultrasensitive MoS_2 phototransistor based on an out of plane MoS_2 PN homojunction. The group mechanically exfoliated MoS_2 to 10 layers and performed electronic doping, using $AuCl_3$ to control the P-type doping of the first few layers. As a result, the device showed extraordinary responsivity and detectivity, although response times in the order of tens of seconds. The responsivity showed values of up to $7 * 10^4$ A/W and a detectivity of $3.5 * 10^{14}$ Jones in the visible and NIR region, shown in Figure 10 (a). MoS_2-based photodetectors can also have outstanding response times, which is very useful for optical communications. Here, Tsai et al. [42] fabricated a tri-layer MoS_2 Schottky metal-semiconductor-metal photodetector with a rise and fall time of 70μs and 110μs, respectively.

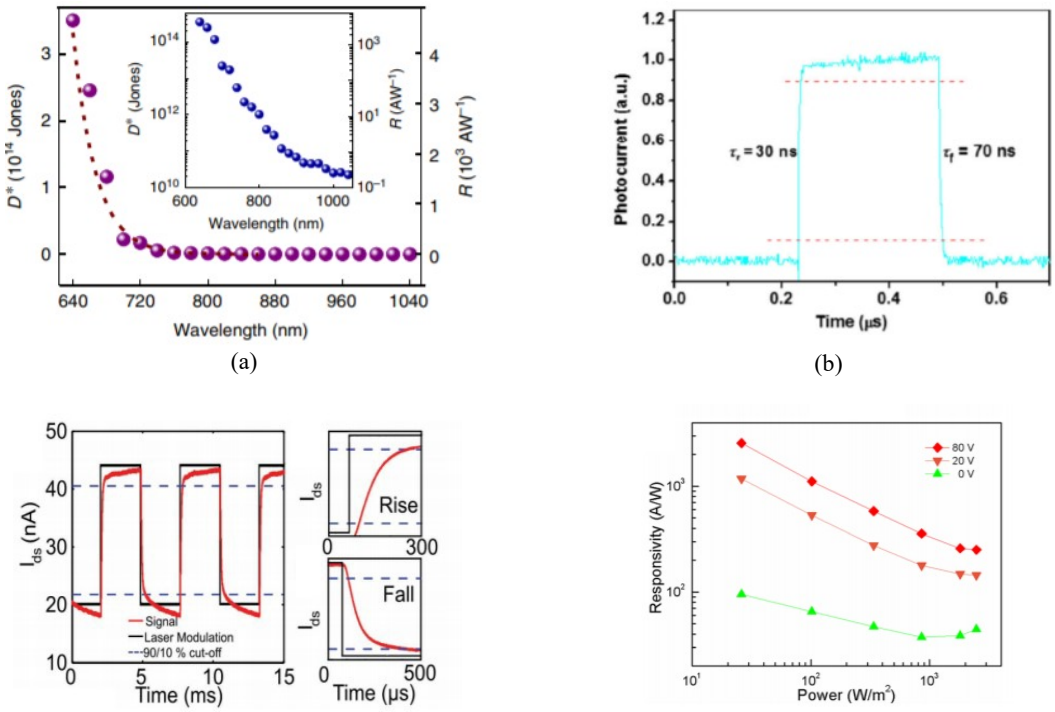

Figure 10: a) Responsivity and detectivity of MoS_2-based photodetector [41]. b) photocurrent over time for a graphene-$MoSe_2$-Si photodetector, demonstrating the response time [46]. c) Photocurrent and rise and fall times of a four-layer $MoTe_2$ FET [38]. d) Responsivity over various biases of few-layered $MoTe_2$ phototransistor [47]

Among MoS_2, other molybdenum chalcogenides have shown good properties useful for photodetectors. Abderrahman et al. [43] synthesized few-layer (about 25 layers) $MoSe_2$ back-gated field effect phototransistor (FET) with a responsivity of 97.1 A/W, which is very high when compared to other MoSe-based photodetectors, but not very good when compared to MoS_2-based detectors reported [41]. However, high detectivity and response time in a $MoSe_2$-based detector have been demonstrated by Mao et al, [44], who used a graphene/$MoSe_2$/Si heterojunction. These authors found a strong detectivity of $7.13 * 10^{10}$ Jones, with a response time as fast as $0.27\mu s$. Regarding fast response speed in $MoSe_2$, it has been shown that $MoSe_2$ monolayer displays a weaker bound exciton peak when observing PL spectra. Thus, $MoSe_2$-based phototransistors can have faster response times than the MoS_2 counterparts [45]. This has been exploited by Geng et al. [46], who produced a $MoSe_2$ nanosheet-based heterojunction (graphene/$MoSe_2$/n-Si) photodetector. Results showed a strong detectivity of about $1.2 * 10^{12}$ Jones, and a response rise and fall time of 30ns and 70ns, respectively, (see Figure 10 (b)). This response time is much faster than most 2D nanostructured photodetectors reported hitherto.

Regarding $MoTe_2$-based devices, while less studied, they show promising figures of merit and performs well when compared to other TMDs. Due to its high mobility and simple fabrication, and lower direct and indirect band gap compared to some other semiconducting TMDs, $MoTe_2$ can have potential in fast, sensitive photodetectors. Octon et al [38] produced a four-layered $MoTe_2$ FET (Figure 9(b)) via mechanical exfoliation and measured the optoelectrical capabilities of the device with and without laser illumination at 685nm. This group found a high responsivity of 6 A/W and a fast response time of 160us (Figure 10(c)) Similarly, Lei Yin et al. [47] fabricated a similar few-layer $MoTe_2$ phototransistor using a carrier tunneling mechanism by using optimized Au contacts to increase electron carrier mobility ($25.2 cm^2V^{-1}s^{-1}$). Using a 473nm laser, the group found a very high responsivity of 2560 A/W for their device at 80V gate voltage (Figure 10 (d)). In addition, studies have utilized the smaller band gap of 2D $MoTe_2$ to detect light in the NIR spectrum for laser sensors and optical communication. Zhang et al. [48] fabricated a graphene-$MoTe_2$-graphene vertical van der Waals heterostructure for NIR photodetection, with decent responsivity of 104mA/W and response times of 24μs for 1064nm detection at zero bias.

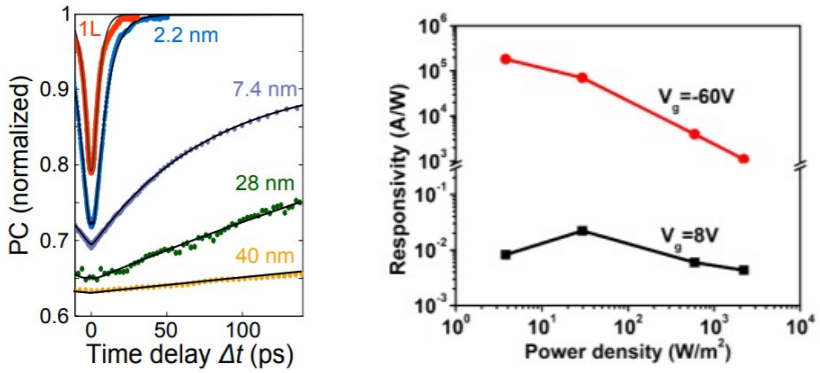

(a) (b)

Figure 11: a) Photocurrent vs time delay for WSe_2-based photodetector with varied thickness (layer number) [51]. b) Responsivity of a monolayer WSe_2 phototransistor [52]

2D tungsten dichalcogenides have also showed strong figures of merit for photodetection using various methods of fabrication. Perea-López et al. [49] produced one of the first tungsten dichalcogenide photodetectors by growing few-layer (about 10 layers) WS_2 flakes via CVD with Au/Ti electrodes. The group found a maximum responsivity of up to 21.2 A/W with response times of about 5.3ms. Since then, the sensitivity of 2D WS_2-based devices has increase dramatically. A high responsivity and detectivity of 1090 A/W and $3.5*10^{11}$ Jones, respectively, have been demonstrated by Gong et al [50]. In order to achieve this, the group fabricated a floating-gate phototransistor using gold nanoparticles (Figure 9 (c)) as the floating gate layer and mechanically exfoliated few-layer WS_2. It was noticed by this group that WS_2 flakes grown by mechanical exfoliation displayed a stronger responsivity and detectivity than those grown by CVD, due to reduced trap densities, which also influenced the group fabrication techniques.

Like WS_2, 2D WSe_2-based detectors have been demonstrated. For example, Massicotte et al. [51] performed time-resolved photocurrent measurements on graphene/Wse_2/graphene heterostructures with various number of layers of WSe_2, encapsulated in hexagonal boron nitride (hBN), another layered material. Their results showed an ultrafast response time of 5.5ps for monolayer devices and responsivity and detectivity as high as 110mA/W and 10^9 Jones for multilayers (7.4 and 28nm thick), respectively. Fewer layers resulted in a lower responsivity and detectivity, but a fast response time, and vice versa. In contrast to WS_2 growth observations affecting the responsivity, CVD-grown WSe_2 monolayer phototransistors were fabricated by Zhang et al. [52] with great success. The group found a responsivity as high as $1.8*10^5$A/W and detectivity of over 10^{14} Jones, which is higher than commercial silicon and InGaAs photodetectors [53].

Various TMD-based optical detectors have been fabricated to utilize the properties of these materials. Table 2 lists the main figures of merit in some of these devices, including Responsivity, Detectivity, response time, EQE, and the wavelength used or wavelength range capable of the detector.

Table 2: various 2D TMD-based devices and figures of merit

Material/type	Responsivity	Detectivity	Response time	EQE	Wavelength	Reference
Monolayer MoS_2 photodetector	3.07 mA/W	-	~1ms	-	633nm	Yang et al [54]
MoS_2 o-n homojunction (~10 layers MoS_2 thick)	7 * 10^4 A/W	$3.5 * 10^{14}$ Jones	~10ms	10%	Vis-NIR	Huo et al [41]
Graphene/$MoSe_2$/Si heterostructure	0.27 A/W	$7.13 * 10^{10}$ Jones	$0.27\mu s$		365-1310nm	Moa et al [44]
Few layer ReS_2 phototransistor (biased)	88600 A/W	$1.182*10^{12}$ Jones	Few to tens of seconds	2*10^7%	532nm	Liu et al [55]
$MoTe_2$ bilayer p-n junction	4.8mA/W	-	~3ns (check)	0.5%	1160nm	Bie et al [56]
Few layer Alpha-$MoTe_2$/MoS_2 heterojunction	322 mA/W	-	25ms	85%	470nm	Pezeski et al [57]
p-WS_2/n-Si 2D/3D heterostructure	1.11 A/W (at -2V)	$5*10^{11}$ Jones (at -2V)	42ms	116%	400-1100nm	Chowdhurry et al [39]
Monolayer MoS_2 phototransistor	880 A/W	-	0.6s	-	561nm (400-680nm range)	Lopez-Sanchez et al [66]
WS_2 monolayer phototransistor	18.8A/W (vacuum) 0.2uA/W (air)	-	<1s (vacuum) <4.5ms (air)	-	-	Lan et al [64]

CONCLUSION

TMDs have been heavily studied over the last decade due to their unique optical properties and applications. Many of these materials have been fabricated by exfoliation and by CVD, thus controlling the sheet size and number of layers. For TMDs the film thickness can be controlled by layer number and that changes the band gap of the material. This change in bandgap will allow, among other properties, to absorb light as we go from UV to NIR of spectrum.

Lee et al. [37] showed how the change in layer number can drastically affect the band gap of MoS_2, finding a change of layers 1, 2, and 3 that resulted in band gaps of 1.35, 1.65, and 1.82eV, respectively. This can also be demonstrated across the other MX_2 materials. Along with pure TMDs such as MoS_2 and WS_2, alloys have also been fabricated, such as $MoWS_2$ and $MoWSe_2$.

The band gap change and high electron carrier mobility allow large tuning of the photodetectors and phototransistors. Stacking various TMDs with graphene to create vertical heterostructures (or van der Waals solids), create new possibilities in responsivity and response time. Responsivity values up to 10^5 A/W [52], and response times in the picosecond range have been demonstrated [51], thus allowing a wide range of light detection for photodetectors and phototransistors.

Many obstacles may arise in future work to push the full possibilities in TMDs. Fabrication issues occur when attempting to make large, high quality TMDs. There may be many issues arise such as long fabrication time, poor quality, or reduced semiconductor properties when optimizing a TMD for a particular application. However, the final product can have many industry applications, as they are currently surpassing commonly used semiconductors. Aside from the challenges ahead, single and few layer TMDs exhibit very promising applications and unique properties.

ACKNOWLEDGEMENT

This work is partially supported by Airforce Office of Scientific Research Grant – FA9550-18-1-0283

REFERENCES

[1] Novoselov, K. S. et al. Electric field effect in atomically thin carbon films. Science 306, 666–669 (2004).

[2] Bhimanapati, G.R., et al., Recent advances in two-dimensional materials beyond graphene. ACS Nano, 2015. 9: p. 11509–11539.

[3] D. W. Latzke, W. Zhang, A. Suslu, T.-R. Chang, H. Lin, H.-T. Jeng, S. Tongay, J. Wu, A. Bansil, A. Lanzara, Electronic structure, spin-orbit coupling, and interlayer interaction in bulk MoS2 and WS2. Phys. Rev. B 91, 235202 (2015).

[4] Gutiérrez, H. R.; Perea-López, N.; Elías, A. L.; Berkdemir, A.; Wang, B.; Lv, R.; López-Urías, F.; Crespi, V. H.; Terrones, M. Extraordinary Room-Temperature Photoluminescence in WS2 Monolayers. Nano Lett. 2012

[5] Tauc, J.; Grigorovici, R.; Vancu, A. Optical properties and electronic structure of amorphous germanium. Phys. Status Solidi 1996, 15, 627–637.

[6] A. O. Slobodeniuk and D. M. Basko, "Exciton-phonon relaxation bottleneck and radiative decay of thermal exciton reservoir in two-dimensional materials," Phys. Rev. B 94, p. 205423, Nov 2016.

[7] Kumar, N. et al. Exciton-exciton annihilation in MoSe2 monolayers. arXiv 1311.1079 (2013).

[8] Palummo, M., Bernardi, M. & Grossman, J. C. Exciton radiative lifetimes in two-dimensional transition metal dichalcogenides. Nano Lett. 15, 2794–2800 (2015)

[9] Winchester, A.; Ghosh, S.; Feng, S.; Elias, A. L.; Mallouk, T.; Terrones, M.; Talapatra, S. Electrochemical Characterization of Liquid Phase Exfoliated Two-Dimensional Layers of Molybdenum Disulfide. ACS Appl. Mater. Interfaces 2014, 6 (3), 2125−2130.

[10] Lezama, I. G.; Ubaldini, A.; Longobardi, M.; Giannini, E.; Renner, C.; Kuzmenko, A. B.; Morpurgo, A. F. Surface Transport and Band Gap Structure of Exfoliated 2h- MoTe2 Crystals. 2D Mater. 2014, 1, 021002.

[11] Morrish, R.; Haak, T.; Wolden, C. A. Low-Temperature Synthesis of n-Type WS2 Thin Films via H2S Plasma Sulfurization of WO3. Chem. Mater. 2014, 26, 3986–3992

[12] Yu, X.; Prevot, M. S.; Guijarro, N.; Sivula, K. Self-Assembled 2D WSe2 Thin Films for Photoelectrochemical Hydrogen Production. Nat. Commun. 2015, 6, 7596.

[13] Lambert J.H. (1760) Photometria sive de mensura et gradibus luminis, colorum et umbrae (Photometry, or, On the measure and gradations of light, colors, and shade) (Augsburg ("Augusta Vindelicorum"), Germany: Eberhardt Klett.

[14] McIntyre, J. D. E.; Aspnes, D. E. Differential Reflection Spectroscopy of Very Thin Surface Films. Surf. Sci. 1971, 24, 417−434. (30) Buckley, R. G.; Beaglehole, D. Absorptance of Thin Films. Appl. Opt. 1977, 16, 2495.

[15] Mak, K. F., M. Y. Sfeir, Y. Wu, C. H. Lui, J. A. Misewich, and T. F. Heinz, 2008, ''Measurement of the Optical Conductivity of Graphene,'' Phys. Rev. Lett. 101, 196405.

[16] Eda G and Maier S A 2013 Two-dimensional crystals: managing light for optoelectronics ACS Nano 7 5660–5

[17] Bernardi, M.; Palummo, M.; Grossman, J. C. Extraordinary Sunlight Absorption and One Nanometer Thick Photovoltaics Using Two-Dimensional Monolayer Materials. Nano Lett. 2013, 13, 3664-3670.

[18] Klots, A. R. et al. Probing excitonic states in suspended two-dimensional semiconductors by photocurrent spectroscopy. Sci. Rep. 4, 6608 (2014).

[19] Britnell, L.; Ribeiro, R.; Eckmann, A.; Jalil, R.; Belle, B.; Mishchenko, A.; Kim, Y.-J.; Gorbachev, R.; Georgiou, T.; Morozov, S., et al. Strong Light-Matter Interactions in Heterostructures of Atomically Thin Films. Science 2013, 340, 1311-1314.

[20] Splendiani, A. et al. Emerging photoluminescence in monolayer MoS2. Nano Lett. 10, 1271–1275 (2010).

[21] Ruppert, C.; Aslan, O. B.; Heinz, T. F. Nano Lett. 2014, 14 (11), 6231−6236.

[22] Li, Y. et al. Measurement of the optical dielectric function of monolayer transition-metal dichalcogenides: MoS2 , MoSe2 , WS2 , and WSe2 . Phys. Rev. B 90, 205422 (2014).

[23] Coehoorn, R., Haas, C. & de Groot, R. A. Electronic structure of MoSe2, MoS2, and WSe2. II. The nature of the optical band gaps. Phys. Rev. B 35, 6203–6206 (1987).

[24] Qiu, D. Y., da Jornada, F. H. & Louie, S. G. Optical Spectrum of MoS2: Many-Body Effects and Diversity of Exciton States. Phys. Rev. Lett. 111, 216805 (2013).

[25] Kozawa, D. et al. Photocarrier relaxation pathway in two-dimensional semiconducting transition metal dichalcogenides. Nat. Commun. 5, 4543 (2014).

[26] M. Bernardi, C. Ataca, M. Palummo and J. C. Grossman, Optical and electronic properties of Two-Dimensional layered materials, Nanophotonics, 2017, 6(2), 479–493.

[27] He, K. et al. Tightly bound excitons in monolayer WSe2. Phys. Rev. Lett. 113,026803 (2014).

[28] Mak, K. F., Lee, C., Hone, J., Shan, J. & Heinz, T. F. Atomically thin MoS2: a new direct-gap semiconductor. Phys. Rev. Lett. 105, 136805 (2010).

[29] Tonndorf, P. et al. Photoluminescence emission and Raman response of monolayer MoS2, MoSe2, and WSe2. Optics Express 21, 4908-4916 (2013).

[30] Conan, A.; Delaunay, D.; Bonnet, A.; Moustafa, A. G.; Spiesser, M. Temperature Dependence of the Electrical Conductivity and Thermoelectric Power in MoTe2 Single Crystals. Phys. Status Solidi B 1979, 94, 279−286.

[31] Böker, T. et al. Band structure of MoS2, MoSe2, and α-MoTe2: angle-resolved photoelectron spectroscopy and ab initio calculations. Phys. Rev. B 64, 235305 (2001)

[32] I. G. Lezama, A. Arora, A. Ubaldini, C. Barreteau, E. Giannini, M. Potemski, A. F. Morpurgo, Indirect-to-Direct Band Gap Crossover in Few-Layer MoTe2, Nano Lett. 15 (2015) 2336-2342

[33] Filler for Zao et al on PL for WS2 and WSe2

[34] E. Torun, H. Sahin, S. Cahangirov, A. Rubio and F. M. Peeters, Anisotropic Electronic, Mechanical, and Optical Properties of Monolayer WTe2, J. Appl. Phys., 2016, 119, 074307, DOI: 10.1063/1.4942162

[35] Amin, B.; Kaloni, T. P.; Schwingenschlogl, U. Strain Engineering of WS2, WSe2, and WTe2. RSC Adv. 2014, 4, 34561–34565.

[36] Zhang, M. et al. Two-dimensional molybdenum tungsten diselenide alloys: photoluminescence, raman scattering, and electrical transport. ACS Nano 8, 7130–7137 (2014).

[37] Lee, H. S. et al. MoS2 nanosheet phototransistors with thickness-modulated optical energy gap. Nano Lett. 12, 446–701 (2012).

[38] Octon, T. J.; Nagareddy, V. K.; Russo, S.; Craciun, M. F.; Wright, C. D. Fast High-Responsivity Few-Layer MoTe2 Photodetectors. Adv. Opt. Mater. 2016, 4, 1750−1754.

[39] Chowdhury R K, Maiti R, Ghorai A, Midya A and Ray S K 2016 Novel silicon compatible p-WS2 2D/3D heterojunction devices exhibiting broadband photoresponse and superior detectivity Nanoscale 8 13429–36

[40] Yin, Z. et al. Single-layer MoS2 phototransistors. ACS Nano 6, 74–80 (2012)

[41] Huo, N.; Konstantatos, G. Ultrasensitive All-2D MoS2 Phototransistors Enabled by An Out-of-Plane MoS2 PN Homojunction. Nat. Commun. 2017, 8, No. 572.

[42] Tsai, D.-S.; Liu, K.-K.; Lien, D.-H.; Tsai, M.-L.; Kang, C.-F.; Lin, C.-A.; Li, L.-J.; He, J.-H. Few Layer MoS2 with Broadband High Photogain and Fast Optical Switching for Use in Harsh Environments. ACS Nano 2013, 7, 3905–3911.

[43] A. Abderrahmane, P. J. Ko, T. V. Thu, S. Ishizawa et al., High photosensitivity few-layered MoSe2 back-gated field-effect phototransistors, Nanotechnology 25 365202 (2014)

[44] Mao, J.; Yu, Y.; Wang, L.; Zhang, X.; Wang, Y.; Shao, Z.; Jie, J. Ultrafast, Broadband Photodetector Based on MoSe2/Silicon Heterojunction with Vertically Standing Layered Structure Using Graphene as Transparent Electrode. Adv. Sci. 2016, 3, 1600018.

[45] Chang, Y. H.; Zhang, W.; Zhu, Y.; Han, Y.; Pu, J.; Chang, J. K.; Hsu, W. T.; Huang, J. K.; Hsu, C. L.; Chiu, M. H. et al. Monolayer MoSe2 Grown by Chemical Vapor Deposition for Fast Photodetection. ACS Nano 2014, 8, 8582-8590

[46] X. Geng, Y. Yu, X. Zhou, C. Wang, K. Xu, Y. Zhang, C. Wu, L. Wang, Y. Jiang and Q. Yang, Design and construction of ultra-thin MoSe2 nanosheet-based heterojunction for highspeed and low-noise photodetection, Nano Res., 2016, 9, 2641–2651.

[47] L. Yin et al. Ultrahigh Sensitive MoTe2 phototransistors driven by carrier tunneling. Appl. Phys. Lett. 108, 043503-1–043503-5 (2016)

[48] K. Zhang, X. Fang, Y. Wang, Y. Wan, Q. Song, W. Zhai, Y. Li, G. Ran, Y. Ye, L. Dai, Ultrasensitive near-infrared photodetectors based on a graphene-MoTe2-graphene vertical Van der Waals heterostructure. ACS Applied Materials and Interfaces 9, 5392-5398 (2017).

[49] Perea-López, N.; Elías, A. L.; Berkdemir, A.; Castro-Beltran, A.; Gutiérrez, H. R.; Feng, S.; Lv, R.; Hayashi, T.; López-Urías, F.; Ghosh, S., et al. Photosensor Device Based on Few-Layered WS2 Films. Adv. Funct. Mater. 2013, 23, 5511–5517.

[50] Y. Gong, J. Lin, X. Wang, G. Shi, S. Lei, Z. Lin, X. Zou, G. Ye, R. Vajtai, B.I. Yakobson, H. Terrones, M. Terrones, Beng K. Tay, J. Lou, S.T. Pantelides, Z. Liu, W. Zhou, P.M. Ajayan, Vertical and in-plane heterostructures from WS2/ MoS2 monolayers, Nat. Mater. 13 (2014) 1135e1142

[51] Massicotte, M. et al. Picosecond photoresponse in van der Waals heterostructures. Nat. Nanotechnol. 11, 42–46 (2016).

[52] Zhang, W.; Chiu, M.-H.; Chen, C.-H.; Chen, W.; Li, L.-J.; Wee, A. T. S. Role of Metal Contacts in High-Performance Phototransistors Based on WSe2 Monolayers. ACS Nano 2014, 8 (8), 8653–8661.

[53] Carey, J. E., Crouch, C. H., Shen, M. & Mazur, E. Visible and near-infrared responsivity of femtosecond-laser microstructured silicon photodiodes. Opt. Lett. 30, 1773–1775 (2005).

[54] Z. Yang, R. Grassi, M. Freitag, Y.-H. Lee, T. Low, and W. Zhu, "Spatial/temporal photocurrent and electronic transport in monolayer molybdenum disulfide grown by chemical vapor deposition," Appl. Phys. Lett. 108(8), 083104 (2016).

[55] Liu, E. et al. High responsivity phototransistors based on few-layer ReS2 for weak signal detection. Nature communication 6, 6991, doi: 10.1038/ncomms7991 (2015).

[56] Bie, Y. Q.; Grosso, G.; Heuck, M.; Furchi, M. M.; Cao, Y.; Zheng, J. B.; Bunandar, D.; Navarro-Moratalla, E.; Zhou, L.; Efetov, D. K.; Taniguchi, T.; Watanabe, K.; Kong, J.; Englund, D.; Jarillo-Herrero, P., A MoTe2-based light-emitting diode and photodetector for silicon photonic integrated circuits. Nat Nanotechnol 2017, 12, 1124.

[57] Pezeshki, A., Shokouh, S. H. H., Nazari, T., Oh, K. & Im, S. Electric and photovoltaic behavior of a few-layer α-MoTe2/MoS2 dichalcogenide heterojunction. Adv. Mater. 28, 3216-3222 (2016)

[58] Yu, H., Cui, X., Xu, X. & Yao, W. Valley excitons in two-dimensional semiconductors. National Science Review 2, 57–70 (2015).

[59] Gmelin, Gmelin handbook of inorganic and organometallic chemistry (SpringerVerlag, Berlin, 1995).

[60] R. Coehoorn, C. Haas, and R. de Groot, “Electronic structure of MoSe2, MoS2, and WSe2. II. The nature of the optical band gaps,” Phys. Rev. B Condens. Matter 35(12), 6203–6206 (1987).

[61] Kuc A, Zibouche N and Heine T 2011 Influence of quantum confinement on the electronic structure of the transition metal sulfide TS${}_{2}$ Phys. Rev. B 83 245213

[62] Yu, W. J.; Liu, Y.; Zhou, H.; Yin, A.; Li, Z.; Huang, Y.; Duan, X. Highly Efficient GateTunable Photocurrent Generation in Vertical Heterostructures of Layered Materials. Nat. Nanotechnol. 2013, 8, 952–958.

[63] F. Gong, W. Luo, J. Wang, P. Wang, H. Fang, D. Zheng, N. Guo, J. Wang, M. Luo, J.C. Ho, X. Chen, W. Lu, L. Liao, W. Hu, High-sensitivity floating-gate phototransistors based on WS2 and MoS2, Adv. Funct. Mater. 26 (2016) 6084e6090

[64] Lan, C., Li, C., Yin, Y. & Liu, Y. Large-area synthesis of monolayer WS2 and its ambient-sensitive photo-detecting performance. Nanoscale 7, 5974–5980 (2015).

[65] Xie C, Mak C, Tao XM, Yan F. Photodetectors based on two-dimensional layered materials beyond graphene. Adv Funct Mater 2017; 27: 1603886.

[66] Lopez-Sanchez, O.; Lembke, D.; Kayci, M.; Radenovic, A.; Kis, A. Ultrasensitive Photodetectors based on Monolayer MoS2. Nat. Nanotechnol. 2013, 8, 497–501.